

Multicomponent mixtures exhibit a vast nucleation-and-growth regime

Yicheng Qiang, Chengjie Luo, and David Zwicker*

Max Planck Institute for Dynamics and Self-Organization, Am Fassberg 17, 37077 Göttingen, Germany

Mixtures of many interacting components can exhibit numerous coexisting droplet types. An exciting example is the cytosol of biological cells, where diverse droplets called condensates are indispensable for cellular function, but it is currently unclear how much their formation is restricted by thermodynamics. Interestingly, linear stability analysis predicts that homogeneous mixtures become more stable with increasing component count. In contrast, we show via numerical simulations and analytical scaling laws that equilibrium states typically contain many coexisting droplets. Combining both results suggests that generic multicomponent mixtures can sustain many stable states with various droplet counts, generalizing the nucleation-and-growth regime of binary mixtures. Our theory also indicates why cells exhibit much fewer condensates than components and how multistability could be leveraged to form condensates independently.

Mixtures with many components are ubiquitous in nature. One particularly interesting case is the cytosol of biological cells, which contains millions of different molecules [1]. Despite this complexity, cells fulfill their function flexibly and robustly. In part, this is because they leverage the physics of multicomponent mixtures to form biomolecular condensates through phase separation [2–7]. However, it is not clear how cells control which condensates form. In particular, it is unclear how much can be attributed to equilibrium thermodynamics and how many condensates are maintained by active processes. Theoretical arguments based on linear stability analysis show that homogeneous states become more stable with larger component counts [8–11], suggesting that the cytosol should stay homogeneous [12]. However, the stability of homogeneous states does not imply that droplets are unstable. In fact, even in binary mixtures, which explain many aspects of condensate formation in cells [2, 13], droplets form even though the homogeneous state is stable in the nucleation-and-growth regime.

The aim of this paper is to generalize the nucleation-and-growth regime to multicomponent mixtures. While the stability of homogeneous states has been discussed before [8–11], phase separated states have been analyzed less thoroughly. This is mainly because computing high-dimensional phase diagrams is challenging [14–16]. To overcome this limitation, we developed a numerical method to detect phase separated equilibrium states. We combine this method with analytical approximations to derive scaling laws for the number of coexisting phases as a function of the interaction strength between components and the overall composition of the system. Our analysis shows that the nucleation-and-growth region generally expands with component count and thus captures the generic behavior of multicomponent mixtures.

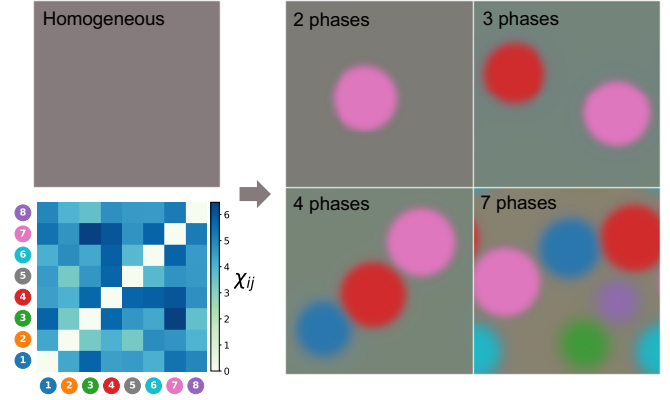


FIG. 1. **Multicomponent mixtures generically exhibit many (meta)stable states with multiple phases.** Five density plots of various stable states of a mixture with $N_c = 8$ components described by the interaction matrix χ_{ij} (lower left) and symmetric average composition ($\bar{\phi}_i = \frac{1}{8}$). Simulation details are described in the Appendix.

Multicomponent mixtures have many stable states

We consider an incompressible, isothermal system comprising N_c different components, each occupying a fraction ϕ_i for $i = 1, \dots, N_c$. In simple cases where these components have equal molecular volumes, lack internal degrees of freedom, and exhibit only pairwise interactions, the thermodynamic behavior is captured by a non-dimensional Flory-Huggins free energy density [17, 18],

$$f(\{\phi_i\}_{i=2}^{N_c}) = \sum_{i=1}^{N_c} \phi_i \ln \phi_i + \frac{1}{2} \sum_{i,j=1}^{N_c} \chi_{ij} \phi_i \phi_j, \quad (1)$$

where $\phi_1 = 1 - \sum_{i=2}^{N_c} \phi_i$. Here, the first term captures translational entropy and the second term accounts for interactions via the symmetric Flory matrix $\chi_{ij} = \chi_{ji}$ with $\chi_{ii} = 0$. Its entries χ_{ij} quantify the interaction energy between species i and j in units of the thermal energy $k_B T$.

We first consider spatially extended volume fraction fields $\phi_i(\mathbf{r}, t)$ in a closed system conserving the aver-

* david.zwicker@ds.mpg.de

age fractions $\bar{\phi}_i = \langle \phi_i(\mathbf{r}, t) \rangle_{\mathbf{r}}$. The corresponding gradient descent dynamics that minimize the overall free energy are given by the Cahn-Hilliard equation [19, 20], $\partial_t \phi_i = \sum_j \nabla \cdot [\Lambda_{ij} \nabla (\partial f / \partial \phi_j - \ell^2 \nabla^2 \phi_j)]$ for $i = 2, \dots, N_c$, where the mobility matrix Λ_{ij} sets time scales and ℓ controls the width of interfaces. Evolving these coupled equations numerically, we find stationary states corresponding to stable configurations of the underlying physical system. Fig. 1 shows an example of a mixture with $N_c = 8$ components, which exhibits a stable homogeneous state (upper left panel). The same system permits at least four different states with various coexisting droplets (right panels). This example demonstrates that multicomponent mixtures can have many stable states with various droplets, even if the homogeneous state is stable. Moreover, the fact that the state with seven phases has the lowest energy suggests that typical equilibrium states exhibit many phases.

To analyze the number of coexisting equilibrium phases in general multicomponent mixtures, we next discuss thermodynamically large systems where phases are homogeneous and the interfaces of width ℓ are negligible. Consequently, equilibrium states minimize the average free energy density \bar{f} of N_p coexisting phases,

$$\bar{f}(N_p, \{J_\alpha\}, \{\phi_i^{(\alpha)}\}) = \sum_{\alpha=1}^{N_p} J_\alpha f(\{\phi_i^{(\alpha)}\}_{i=2}^{N_c}), \quad (2)$$

where phase α is described by its composition $\phi_i^{(\alpha)}$ and relative volume J_α under the volume constraint $\sum_{\alpha=1}^{N_p} J_\alpha = 1$ and the fixed average volume fractions $\bar{\phi}_i = \sum_{\alpha=1}^{N_p} J_\alpha \phi_i^{(\alpha)}$. Given an interaction matrix χ_{ij} and average composition $\bar{\phi}_i$, we can thus in principle minimize \bar{f} to obtain the phase count N_p together with the fractions of volume J_α and compositions $\phi_i^{(\alpha)}$ of all phases.

Realistic multicomponent systems have a wide distribution of compositions $\bar{\phi}_i$ and interactions strengths χ_{ij} . To obtain generic results, we focus on general features of χ_{ij} by parameterizing the typical interaction strength and its variability, i.e., we draw the entries χ_{ij} for $i < j$ independently from the normal distribution $\mathcal{N}(\bar{\chi}, \sigma_\chi)$, parameterized by the mean interaction $\bar{\chi}$ and the standard deviation σ_χ . In particular, this choice allows direct comparison with previous results on the stability of homogeneous states [8–11]. To capture variability in composition, we consider two extreme cases, where the average fraction is either the same for all components ($\bar{\phi}_i = 1/N_c$) or distributed uniformly (obeying $\sum_{i=1}^{N_c} \bar{\phi}_i = 1$). The first choice provides more intuitive results that we can compare to previous works [8, 11], whereas the latter choice captures some variability of realistic systems. For both choices, we will quantify the average phase count \bar{N}_p and the stability of the homogeneous state as functions of N_c , $\bar{\chi}$, and σ_χ .

Symmetric mixtures exhibit discrepancy between equilibrium and stability of homogeneous states

To build intuition, we start with the special case of identical interactions ($\chi_{i \neq j} = \bar{\chi}$, $\sigma_\chi = 0$) and symmetric compositions ($\bar{\phi}_i = 1/N_c$). We first determine when the homogeneous state is unstable, which is the case when the Hessian matrix $\mathbf{H} = \{H_{ij}\}_{i,j=2}^{N_c}$ with $H_{ij} = \partial^2 f / \partial \bar{\phi}_i \partial \bar{\phi}_j$ is no longer positive definite, i.e., where at least one eigenvalue is negative. For $\chi_{i \neq j} = \bar{\chi}$ and $\bar{\phi}_i = 1/N_c$, the Hessian simplifies to $H_{ij} = (\delta_{ij} + 1)(N_c - \bar{\chi})$. The unique eigenvalues, $N_c - \bar{\chi}$ and $N_c(N_c - \bar{\chi})$, are negative when

$$\bar{\chi} > N_c. \quad (3)$$

If this condition is fulfilled, the homogeneous state is unstable and phase separation is inevitable.

Phase separation can happen even when the homogeneous state is (locally) stable [21, 22]. To determine when this is the case, we next discuss equilibrium states, which minimize the free energy density \bar{f} given by Eq. (2). In the symmetric case considered in this section, the only possible phase separated state is the one where N_c phases coexist, each concentrating one component to a high fraction ϕ^+ while diluting the others to $\phi^- = (1 - \phi^+) / (N_c - 1)$. Consequently, the minimal interaction strength to have phase separation can be determined numerically by comparing the free energy of this phase separated state with the homogeneous state. To get an estimate for the minimal interaction strength, we use a variational principle and identify a candidate state with lower energy than the homogeneous state: Since the state where each of the N_c phases enriches exactly one component ($\phi^+ = 1, \phi^- = 0$) has $\bar{f} = 0$, phase separation must happen when the homogeneous state has $\bar{f} > 0$, implying the sufficient condition

$$\bar{\chi} > \frac{2N_c}{N_c - 1} \ln N_c. \quad (4)$$

Fig. A1 shows that Eq. (4) provides a good approximation for the numerically determined critical value of $\bar{\chi}$, especially for large N_c . A more detailed analysis presented in the Appendix shows that the diluted components have the fraction

$$\phi^-(N_c) \approx -\frac{W_0[-e^{-\bar{\chi}}(N_c(\bar{\chi} - 1) + 1)]}{N_c(\bar{\chi} - 1) + 1} \stackrel{\bar{\chi} \gg 1}{\approx} e^{-\bar{\chi}}, \quad (5)$$

where $W_0(r)$ is the principal branch of the Lambert W function satisfying $W(r)e^{W(r)} = r$. The limit for large $\bar{\chi}$ shows that dilute fractions are suppressed exponentially.

These results confirm the expectation that stronger repulsion (i.e., larger $\bar{\chi}$) destabilize the homogeneous state (Eq. (3)), induce phase separation (Eq. (4)), and enhance the compositional differences between phases (Eq. (5)). However, comparing Eqs. (3) and (4) reveals a huge discrepancy between the stability analysis and equilibrium: While the typical interaction $\bar{\chi}$ needs to scale with the component count N_c to destabilize the homogeneous

state, phase separation is already possible when $\bar{\chi}$ scales only logarithmically with N_c . These scalings suggest that the parameter region where the homogeneous state is stable and the equilibrium state exhibits phase separation (corresponding to the nucleation-and-growth regime) expands with larger component count N_c .

Compositional variation maintains the discrepancy

Phase separation of multicomponent mixtures not only depends on interactions but also composition [11]. We thus next test how compositional variations affect the discrepancy between unstable homogeneous states and equilibrium. To capture compositional variations in an unbiased way, we average over all permissible volume fractions ($\bar{\phi}_i \geq 0$, $\sum_{i=1}^{N_c} \bar{\phi}_i = 1$), maintaining identical interactions for now ($\chi_{i \neq j} = \bar{\chi}$, $\sigma_\chi = 0$). Since this system is more variable than the one discussed above, we can distinguish various degrees of instability of the homogenous state by counting the number of negative eigenvalues of the Hessian \mathbf{H} , denoted as the number of unstable modes, N_u . If the homogeneous state is the equilibrium state, we necessarily have $N_u = 0$ and $N_p = 1$. In contrast, for very strong phase separation, the homogeneous state will be maximally unstable, $N_u = N_c - 1$, and the phase count assumes the maximal value $N_p = N_c$ allowed by Gibbs phase rule [23]. In both extremes we have $N_p = N_u + 1$, but these two values might deviate from each other substantially in intermediate parameter regions. To quantify this behavior, we next study the mean values \bar{N}_p and $\bar{N}_u + 1$ averaged over all permissible compositions.

To determine the average number of unstable modes, \bar{N}_u , we diagonalized the Hessian matrix \mathbf{H} numerically for many different compositions, sampled uniformly over the entire phase diagram [24]. Fig. 2a shows that \bar{N}_u increases with the mean interaction strength $\bar{\chi}$, as expected. An analytical estimate for \bar{N}_u follows from Cauchy's interlacing theorem [25]: The number N_u of negative eigenvalues of \mathbf{H} equals the number of sign changes in the sequence

$$\det \mathbf{H}_0, \det \mathbf{H}_1, \dots, \det \mathbf{H}_{N_c-1}, \quad (6)$$

where $\det \mathbf{H}_n$ is the determinant of the rank- n leading minor of \mathbf{H} . For identical interactions ($\chi_{i \neq j} = \bar{\chi}$), we obtain $\det \mathbf{H}_n = (\prod_{i=1}^{n+1} q_i)(\sum_{i=1}^{n+1} q_i^{-1})$ with $q_i = \bar{\phi}_i^{-1} - \bar{\chi}$. The number of sign changes in (6) is thus either N_- or $N_- - 1$, where N_- is the number of negative q_i , since each negative q_i contributes one sign change in the product $\prod_{i=1}^{n+1} q_i$ when varying n , while a potential sign change of the second factor, $\sum_{i=1}^{n+1} q_i^{-1}$, cancels at most one sign change; see Appendix for a detailed derivation. Since N_- simply counts how many $\bar{\phi}_i$ are larger than $\bar{\chi}^{-1}$, \bar{N}_u is bounded by $E_{N_c}[\bar{\phi}_i > \bar{\chi}^{-1}] \leq \bar{N}_u + 1 \leq E_{N_c}[\bar{\phi}_i > \bar{\chi}^{-1}] + 1$, where $E_{N_c}[\bar{\phi}_i > h] = N_c(1-h)^{N_c-1}$ denotes the expected number of $\bar{\phi}_i$ larger than h when $\bar{\phi}_i$ is drawn randomly on the phase diagram. Taken together, the

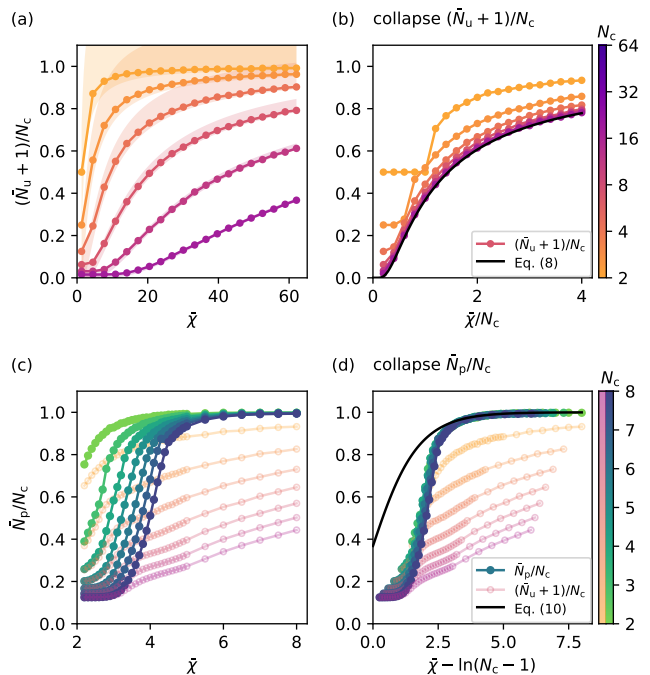


FIG. 2. **Average number of phases exceeds number of unstable modes for identical interactions.** (a, b) Normalized average number of unstable modes, $(\bar{N}_u + 1)/N_c$, as a function of the mean interaction strength $\bar{\chi}$ in (a) and the scaled interaction $\bar{\chi}/N_c$ in (b) for various component counts N_c . The shaded area in (a) indicates the bounds given by Eq. (7), and the black line in (b) marks the asymptotic expression (8). (c, d) Normalized average number of coexisting phases, \bar{N}_p/N_c , (green-blue) and $(\bar{N}_u + 1)/N_c$ (orange-purple) as a function of $\bar{\chi}$ in (c) and $\bar{\chi} - \ln(N_c - 1)$ in (d). The black line in (d) marks the asymptotic expression (10). (a-d) Each dot results from an average over 500–20 000 uniformly sampled compositions.

normalized average number of unstable modes, $(\bar{N}_u + 1)/N_c$, is bounded by

$$\left(1 - \frac{1}{\bar{\chi}}\right)^{N_c-1} \leq \frac{\bar{N}_u + 1}{N_c} \leq \left(1 - \frac{1}{\bar{\chi}}\right)^{N_c-1} + \frac{1}{N_c}, \quad (7)$$

consistent with numerical data (Fig. 2a). The two bounds in Eq. (7) converge for large N_c , implying

$$\frac{\bar{N}_u + 1}{N_c} \underset{N_c \gg 1}{\approx} \left(1 - \frac{1}{\bar{\chi}}\right)^{N_c-1} \underset{\bar{\chi} \gg 1}{\approx} e^{-N_c/\bar{\chi}}. \quad (8)$$

The limit on the right suggests that the normalized number of unstable modes averaged over the phase diagram, $(\bar{N}_u + 1)/N_c$, only depends on the single scaled interaction parameter $\bar{\chi}/N_c$. The data collapse shown in Fig. 2b indeed confirms this scaling for $N_c \gtrsim 16$.

To test how well the average number \bar{N}_u of unstable modes predicts the average phase count, \bar{N}_p , we next investigate equilibrium states by minimizing the mean free energy \bar{f} given by Eq. (2). We designed an efficient

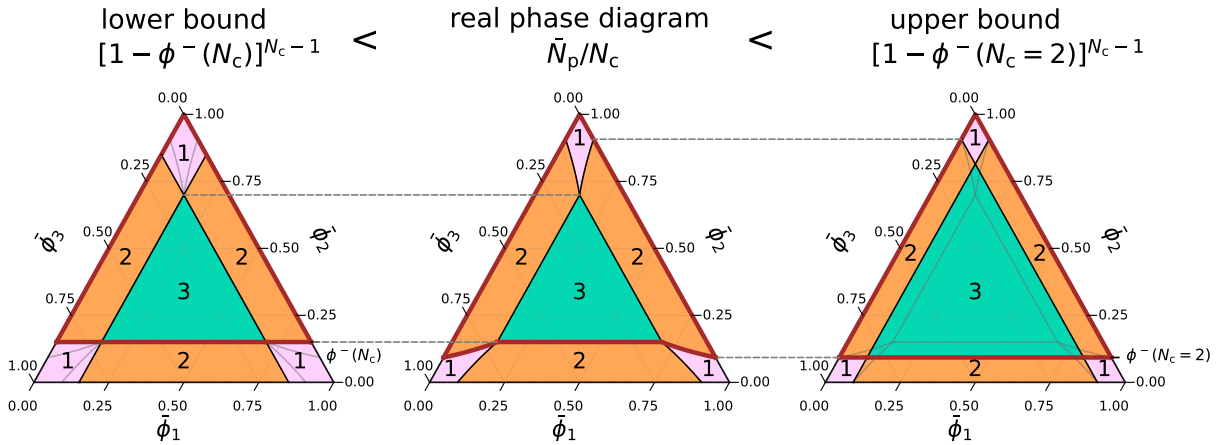


FIG. 3. **Illustration of phase count bounds.** The central panel shows the phase diagram as a function of the volume fractions ϕ_i of $N_c = 3$ components for $\chi_{i \neq j} = 2.8$. The colored regions indicate the number of coexisting phases, $N_p = 1, 2, 3$. The adjacent panels approximate the phase diagram using boundaries parallel to the axes, obtained by expanding the $N_p = 1$ region (left) and the central region with $N_p = N_c$ (right). They respectively provide lower and upper bounds to the average phase count \bar{N}_p , which can be obtained from the fraction covered by an area associated with each component (thick red lines). The average phase count \bar{N}_p for the three panels is 2.17, 2.22, and 2.47 (from left to right).

algorithm to determine coexisting phases at arbitrary interactions and mean compositions [26], which is similar to the Gibbs ensemble method [27–30]. The method minimizes \bar{f} by redistributing components and volumes across an ensemble of compartments, while obeying volume and material conservation; see Appendix for the numerical details. In a key improvement over our earlier implementation [16, 24], we now initialize compartments such that the average fractions $\bar{\phi}_i$ can attain any value, which in principle allows us to determine the full $(N_c - 1)$ -dimensional phase diagram. Sampling the obtained phase count N_p uniformly over the entire phase diagram allows us to estimate the average number of coexisting phases, \bar{N}_p , in equilibrium.

The numerical results shown in Fig. 2c indicate that \bar{N}_p increases much more quickly as a function of the interaction strength $\bar{\chi}$ than the number of unstable modes \bar{N}_u . Moreover, the scaled interaction strength $\bar{\chi}/N_c$, derived for \bar{N}_u from Eq. (8), cannot collapse these data. To derive an alternative scaling law, we focus on strong interactions, where Eq. (4) is satisfied, so we have the maximal number of phases ($N_p = N_c$) for equal composition at the center of the phase diagram ($\bar{\phi}_i = 1/N_c$). The region where these N_c phases are stable forms a $(N_c - 1)$ -dimensional simplex (green region in Fig. 3), which covers a larger area for higher $\bar{\chi}$. While fewer phases are observed outside this region, the symmetric structure of the phase diagram still allows us to determine the average phase count \bar{N}_p . In essence, the phase diagram has a three-fold rotational symmetry, so we can focus on one primitive region (highlighted by the red outlines in Fig. 3). Since the phase count at each point in the phase diagram equals the number of (symmetric) primitive regions covering that point, \bar{N}_p/N_c is simply given by the fraction of the phase diagram covered by a single

primitive region. We next derive lower and upper bounds by approximating the primitive region by inscribed and circumscribed simplexes. For the example shown in the central panel of Fig. 3, we thus replace the lower boundary of the primitive region by a straight line coinciding with the boundary of the central three-phase region (left panel in Fig. 3). The composition of the three-phase region is $\phi^-(N_c)$ given by Eq. (5), so the relative area of the simplex is given by $[1 - \phi^-(N_c)]^{N_c - 1}$. In contrast, for the upper bound we replace the boundary by a straight line anchored at the corner points of the primitive region (right panel in Fig. 3). The corresponding fraction is $\phi^-(N_c = 2)$ since the edge of the phase diagram corresponds to a binary system. These arguments generalize to higher dimensions, so the normalized average phase count \bar{N}_p/N_c is generally bounded by

$$[1 - \phi^-(N_c)]^{N_c - 1} \leq \frac{\bar{N}_p}{N_c} \leq [1 - \phi^-(N_c = 2)]^{N_c - 1}. \quad (9)$$

The fraction $\phi^-(N_c)$ given by Eq. (5) converges to $e^{-\bar{\chi}}$ for all N_c if $\bar{\chi} \gg 1$, so

$$\frac{\bar{N}_p}{N_c} \stackrel{\bar{\chi} \gg 1}{\approx} (1 - e^{-\bar{\chi}})^{N_c - 1} \approx \exp[-(N_c - 1)e^{-\bar{\chi}}]. \quad (10)$$

This approximation reveals that \bar{N}_p is asymptotically given by $E_{N_c}[\bar{\phi}_i > e^{-\bar{\chi}}]$, i.e., the expected number of $\bar{\phi}_i$ larger than $e^{-\bar{\chi}}$. This result is similar to that for \bar{N}_u following from Eq. (8), except the threshold is now $1/e^{\bar{\chi}}$ instead of $1/\bar{\chi}$, implying an exponential scaling when switching from stability analysis to equilibrium.

Using Eq. (10), we predict that \bar{N}_p/N_c is governed by the single shifted interaction parameter $\bar{\chi} - \ln(N_c - 1)$. Indeed, Fig. 2d shows that this scaling collapses the data in a surprisingly large parameter range, even when the

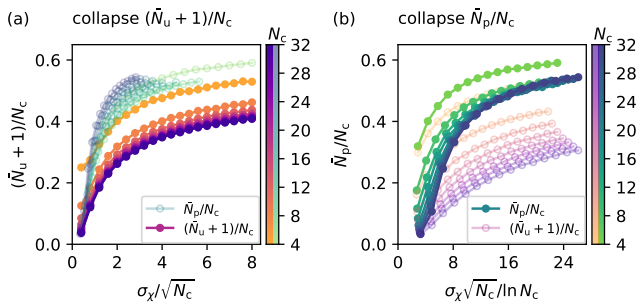


FIG. 4. **More variable interactions elicit more phases.** Normalized average number of unstable modes, $(\bar{N}_u + 1)/N_c$ (orange-purple), and normalized average number of coexisting phases, \bar{N}_p/N_c (green-blue), as a function of two different scalings of the standard deviation σ_χ of the interactions for various component counts N_c and $\bar{\chi} = 0$. Each dot results from an average over 10^3 – 10^4 randomly chosen pairs of interaction matrices χ_{ij} and compositions $\bar{\phi}_i$.

limits used to derive Eq. (10) are violated. The data collapse that we identify in Fig. 2d indicates that the interaction parameter $\chi_{i \neq j} = \bar{\chi}$ needs to exceed roughly $3 + \ln(N_c - 1)$ to have many phases ($\bar{N}_p \approx N_c$). In contrast, the stability analysis predicted a linear scaling of $\bar{\chi}$ with N_c , so that the discrepancy between the phase count and the number of unstable modes increases with larger component count N_c .

Random interactions maintain the discrepancy

Beside compositional variations realistic mixtures exhibit large variations in the strength of the pairwise interaction between components. To test whether variable interactions affect the discrepancy between unstable homogeneous states and equilibrium, we next consider random interaction matrices χ_{ij} .

For simplicity, we first vary only the standard deviation σ_χ of the normal distribution governing the symmetric interaction matrix χ_{ij} while keeping a vanishing mean interaction ($\bar{\chi} = 0$). For symmetric compositions ($\bar{\phi}_i = 1/N_c$), \bar{N}_u can be obtained by treating the Hessian \mathbf{H} as a random matrix. In particular, \mathbf{H} consists of an enthalpic part given by the random χ_{ij} matrix and an entropic part given by a diagonal matrix with $\bar{\phi}_i^{-1}$ on the diagonal. The corresponding eigenvalues read $\lambda_i + \bar{\phi}_i^{-1}$, where the distribution of eigenvalues λ_j of χ_{ij} forms a semicircle of radius of $2\sigma_\chi\sqrt{N_c}$ centered at the origin [8]. In particular, the average number of negative eigenvalues is then $\bar{N}_u = E_{N_c}[\lambda_j > \bar{\phi}_i^{-1}]$. Geometrically, the fraction of the average number of unstable modes, \bar{N}_u/N_c , thus equals the fraction of the semicircle right of $\bar{\phi}_i^{-1}$, which is a function of the single parameter $\sigma_\chi\sqrt{N_c}/\bar{\phi}_i^{-1} = \sigma_\chi N_c^{-1/2}$. This scaling even persists for random compositions $\bar{\phi}_i$ [11], where the above analysis does not hold. Fig. 4a confirms that this scaling collapses

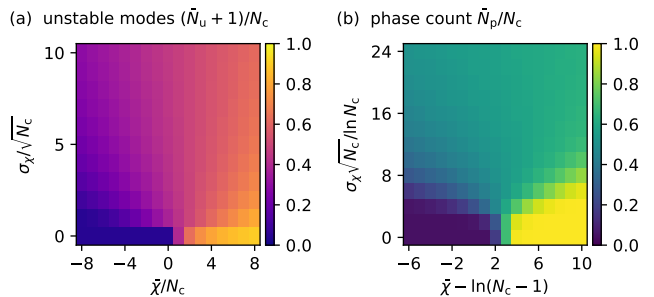


FIG. 5. **Summary of scaling functions.** (a) Normalized average number of unstable modes, $(\bar{N}_u + 1)/N_c$, as a function of scaled mean interaction $\bar{\chi}$ and standard deviation σ_χ . (b) Normalized average number of coexisting phases, \bar{N}_p/N_c , as a function of scaled $\bar{\chi}$ and σ_χ . (a, b) The shown master functions were obtained by averaging 300 samples of random interaction matrices and compositions for each value of $\bar{\chi}$ and σ_χ for component counts $N_c = 16, 20, 24, 28, 32$.

data for \bar{N}_u , whereas it fails for the phase counts \bar{N}_p that we determined using our numerical algorithm.

To also obtain a scaling relation for the phase count \bar{N}_p , we exploit an analogy between \bar{N}_u and \bar{N}_p that we derived above for identical interactions ($\chi_{i \neq j} = \bar{\chi}$): We found $\bar{N}_u \sim E_{N_c}[\bar{\chi} > \bar{\phi}_i^{-1}]$ and $\bar{N}_p \sim E_{N_c}[e^{\bar{\chi}} > \bar{\phi}_i^{-1}]$, indicating that the two quantities only differ in the dependence on $\bar{\chi}$ in the argument. For random interactions, we thus speculate that the scaling of \bar{N}_p can be inferred from the result for \bar{N}_u by substituting e^{λ_i} for the eigenvalues λ_i . This procedure suggests that \bar{N}_p/N_c can be expressed as a function of the scaling parameter $\sigma_\chi\sqrt{N_c}/\ln N_c$ for sufficiently large N_c , which is confirmed by the data collapse shown in Fig. 4b. Thus, larger variations σ_χ of the interactions generally lead to more phases, and \bar{N}_p/N_c even grows with N_c when σ_χ is fixed. In contrast, the stability analysis suggests that σ_χ needs to grow with $\sqrt{N_c}$ to have the same fraction of unstable modes, so \bar{N}_u severely underestimates the phase count \bar{N}_p , particularly for large N_c .

We next test how a non-zero mean interaction $\bar{\chi}$ affects the obtained scalings. Combining the scalings obtained for identical interactions ($\sigma_\chi = 0$) and vanishing mean interactions ($\bar{\chi} = 0$), we postulate the average number of unstable modes and phase count respectively scale as

$$\frac{\bar{N}_u + 1}{N_c} \approx g_u \left(\frac{\bar{\chi}}{N_c}, \frac{\sigma_\chi}{\sqrt{N_c}} \right) \quad \text{and} \quad (11a)$$

$$\frac{\bar{N}_p}{N_c} \approx g_p \left(\bar{\chi} - \ln(N_c - 1), \frac{\sigma_\chi\sqrt{N_c}}{\ln N_c} \right), \quad (11b)$$

where g_u and g_p are the associated master functions, which we determine numerically (Fig. 5). The deviation of the actually measured data to this prediction is generally low (see Fig. A2), implying that the proposed scaling captures the dominant behavior. The master functions shown in Fig. 5 are qualitatively similar: For strongly attractive interactions (large negative $\bar{\chi}$ and small σ_χ),

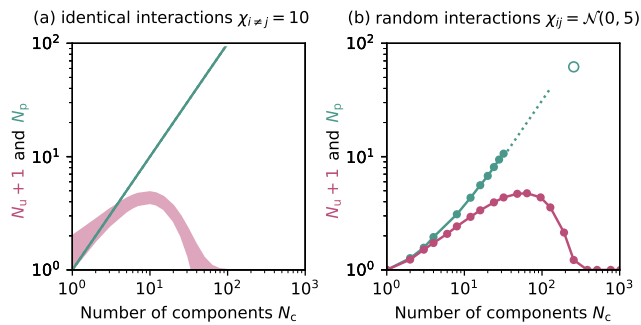


FIG. 6. **Mixtures can have many coexisting phases and stable homogeneous states.** (a) Analytical estimates of average number of coexisting phases \bar{N}_p (green line, Eq. (9)) and average number of unstable modes \bar{N}_u (red region, Eq. (7)) as a function of component count N_c for mixtures with identical interactions ($\chi_{i \neq j} = 10$). (b) Numerically determined \bar{N}_p (green dots) and \bar{N}_u (red dots) as a function of N_c for random interactions ($\bar{\chi} = 0$, $\sigma_\chi = 5$). The green dotted line shows a linear extrapolation toward the single data point at $N_c = 256$ (open circle).

they are close to 0, implying that only very few phases form. In contrast, when repulsive interactions dominate (large $\bar{\chi}$ and small σ_χ), the master functions converge to 1, implying N_c phases coexist. For strongly varying interactions (small $\bar{\chi}$ and large σ_χ), both master functions converge to $\frac{1}{2}$ and the respective influence of $\bar{\chi}$ can be approximated analytically; see Appendix. While the master functions exhibit similarities, the axes are scaled very differently, implying different interpretations of what constitutes large interactions: For large N_c , the mean interactions $\bar{\chi}$ and the variance σ_χ^2 need to scale with N_c to obtain similar fractions \bar{N}_u/N_c of unstable modes. In contrast, the predicted phase count \bar{N}_p exhibits a much weaker dependence on N_c : For instance, the influence of N_c on the mean interaction is only logarithmically. Moreover, the predicted fraction \bar{N}_p/N_c increases with N_c even if σ_χ is kept constant. These scaling laws also hold for different samplings of the compositions (see Appendix) and are thus likely robust. In particular, we conclude that the observed discrepancy between N_p and N_u reflects a general behavior of multicomponent mixtures.

Multicomponent mixtures exhibit a large nucleation-and-growth regime

The scaling laws given in Eq. (11) allow us to speculate about the number N_u of unstable modes and the equilibrium phase count N_p in realistic systems. We here focus on biological cells, where a typical interaction strength is a few $k_B T$, but the actual component count N_c can vary over several orders of magnitude; there are an estimated number of 10^5 different proteins [1]. For such a scenario, numerical data indicates that the homogeneous state becomes more stable (\bar{N}_u approaches 0) [12], whereas the

expected phase count in equilibrium increases linearly with N_c for identical interactions (Fig. 6a) and randomly distributed interactions (Fig. 6b). This behavior can be understood based on the scaling laws given in Eq. (11): For large N_c at fixed $\bar{\chi}$ and σ_χ , the fraction of unstable modes approaches $g_u(0, 0) = 0$. In contrast, the governing parameters for N_p scale much slower, keeping the phase count fraction almost constant in a wide range of N_c . The number N_p of coexisting phases would only decrease at much larger values of N_c , implying that there is a larger parameter regime where the homogeneous state is stable while the equilibrium state exhibits many phases, consistent with the example shown in Fig. 1.

The discrepancy between the number of unstable modes and the equilibrium phase count generalizes the familiar nucleation-and-growth regime in binary mixtures. Even in binary mixtures, the fraction beyond which phase separation sets in (the binodal) is approximately given by $e^{-\chi}$, whereas the homogeneous state only becomes unstable for fractions larger than $\frac{1}{2}\chi^{-1}$ (the spinodal) [20, 31]. These scalings are consistent with the respective exponential and linear scalings that we revealed above, but we additionally find a strong influence of the component count N_c . Since N_c sets the dimensionality of the phase diagram, we speculate that its influence is of geometric origin: The region where the homogeneous state is stable typically occupies the central region of the phase diagram, so multi-stability is only possible for parameters close to the boundaries of the phase diagram. The fraction of the phase diagram that is close to the boundary increases dramatically with dimension, suggesting that the behavior at the boundary will dominate.

Discussion

We showed that multicomponent mixtures generally exhibit many more phases than one would expect from a linear stability analysis of homogeneous states. While already binary mixtures show this discrepancy in the form of the nucleation-and-growth regime, adding more components amplifies this behavior. The fact that equilibrium states can exhibit many phases even when the homogeneous state is stable further suggests that there are additional stable states with fewer droplets. Since we only considered passive systems governed by equilibrium thermodynamics, these states must be separated by energy barriers, which could be overcome by nucleation. We thus expect that starting from the stable homogeneous state several different types of droplets can be nucleated independently of each other, giving rise to a sequence of states with increasing droplet counts (Fig. 1). Experimentalists begin to analyze such behaviors [32], but there are many open questions, including the number of stable states, the magnitude of energy barriers, and whether there is a hierarchy of nucleation.

Our theory predicts two fundamental aspects of phase separation inside biological cells. First, the fact that cells

comprise millions of different components with weak interactions on the scale of the thermal energy $k_B T$ suggests that the equilibrium phase count is small compared to the component count (lower left corner of Fig. 5B), which is consistent with the observed $10^1 \dots 10^3$ different condensates [33] that form from $10^5 \dots 10^7$ different biomolecules [1]. Second, our theory implies multistability, which cells could exploit to create and remove different droplets independently of each other to fulfill separate functions robustly. However, there is also the exciting possibility that formation of different droplets is coupled, which might be functionally relevant. In both cases, cells could fine-tune the interactions of molecules, e.g., through evolutionary adaptation of the respective genes, even though our theory suggests that such fine-tuning is not necessary to obtain many multi-stable droplets. Moreover, active processes would allow cells to exert finer control on when droplets form and how large they get [20, 22, 34–36]. Taken together, our theory paints a picture of a multi-stable cytosol where hundred types of condensates can coexist independently.

We validated our scaling laws against numerical data, although the computational complexity limits the maximally attainable component count N_c . While most scaling laws were derived based on analytical estimates, the dependence of the phase count \bar{N}_p on the interaction vari-

ance σ_χ^2 was only obtained by analogy and might thus break down beyond the tested regime. We here also focused on interactions that are randomly distributed with little structure, whereas realistic systems will likely have higher-order [37] and structured interactions [38–40], e.g., arising from evolutionary optimization, which affects phase separation [41, 42]. Moreover, the composition of various components is typically broadly distributed, which might affect accessible phases. To address these aspects, a detailed understanding of the geometry of phase space would be helpful, which certainly warrants further investigations and experimental validation. Our results on the generic behavior of multicomponent mixtures, and particularly the numerical method to determine coexisting phases, will guide future research in these directions.

ACKNOWLEDGMENTS

We thank Thomas Michaels, Filipe Thewes, and Peter Sollich for helpful discussions. We thank Filipe Thewes and Gerrit Wellecke for critical reading of the manuscript. We gratefully acknowledge funding from the Max Planck Society and the European Union (ERC, EmulSim, 101044662).

-
- [1] G. M. Cooper and K. Adams, *The Cell: A Molecular Approach* (Oxford University Press, 2022).
- [2] A. A. Hyman, C. A. Weber, and F. Jülicher, Liquid-Liquid Phase Separation in Biology, *Annual Review of Cell and Developmental Biology* **30**, 39 (2014).
- [3] S. F. Banani, H. O. Lee, A. A. Hyman, and M. K. Rosen, Biomolecular condensates: Organizers of cellular biochemistry, *Nat Rev Mol Cell Biol* **18**, 285 (2017).
- [4] W. M. Jacobs and D. Frenkel, Phase Transitions in Biological Systems with Many Components, *Biophysical Journal* **112**, 683 (2017).
- [5] P. Sartori and S. Leibler, Lessons from equilibrium statistical physics regarding the assembly of protein complexes, *Proc. Natl. Acad. Sci. U.S.A.* **117**, 114 (2020).
- [6] D. L. J. Lafontaine, J. A. Riback, R. Bascetin, and C. P. Brangwynne, The nucleolus as a multiphase liquid condensate, *Nat Rev Mol Cell Biol* **22**, 165 (2021).
- [7] C. A. Azaldegui, A. G. Vecchiarelli, and J. S. Biteen, The emergence of phase separation as an organizing principle in bacteria, *Biophysical Journal* **120**, 1123 (2021).
- [8] R. P. Sear and J. A. Cuesta, Instabilities in Complex Mixtures with a Large Number of Components, *Phys. Rev. Lett.* **91**, 245701 (2003).
- [9] W. M. Jacobs and D. Frenkel, Predicting phase behavior in multicomponent mixtures, *The Journal of Chemical Physics* **139**, 024108 (2013).
- [10] K. Shrinivas and M. P. Brenner, Phase separation in fluids with many interacting components, *Proc. Natl. Acad. Sci. U.S.A.* **118**, e2108551118 (2021).
- [11] F. C. Thewes, M. Krüger, and P. Sollich, Composition Dependent Instabilities in Mixtures with Many Components, *Phys. Rev. Lett.* **131**, 058401 (2023).
- [12] R. P. Sear, The cytoplasm of living cells: A functional mixture of thousands of components, *J. Phys.: Condens. Matter* **17**, S3587 (2005).
- [13] J. Berry, C. P. Brangwynne, and M. Haataja, Physical principles of intracellular organization via active and passive phase transitions, *Rep. Prog. Phys.* **81**, 046601 (2018).
- [14] S. Mao, D. Kuldinow, M. P. Haataja, and A. Košmrlj, Phase behavior and morphology of multicomponent liquid mixtures, *Soft Matter* **15**, 1297 (2019).
- [15] S. Mao, M. S. Chakraverti-Wuerthwein, H. Gaudio, and A. Košmrlj, Designing the Morphology of Separated Phases in Multicomponent Liquid Mixtures, *Phys. Rev. Lett.* **125**, 218003 (2020).
- [16] W. M. Jacobs, Theory and Simulation of Multiphase Coexistence in Biomolecular Mixtures, *J. Chem. Theory Comput.* **19**, 3429 (2023).
- [17] P. J. Flory, Thermodynamics of High Polymer Solutions, *J. Chem. Phys.* **10**, 51 (1942).
- [18] M. L. Huggins, Solutions of Long Chain Compounds, *J. Chem. Phys.* **9**, 440 (1941).
- [19] J. W. Cahn and J. E. Hilliard, Free Energy of a Nonuniform System. I. Interfacial Free Energy, *J. Chem. Phys.* **28**, 258 (1958).
- [20] D. Zwicker, O. W. Paulin, and C. ter Burg, *Physics of droplet regulation in biological cells* (2025), [arXiv:2501.13639](https://arxiv.org/abs/2501.13639) [physics].
- [21] L. P. McMaster, Aspects of Polymer-Polymer Thermodynamics, *Macromolecules* **6**, 760 (1973).
- [22] D. Zwicker, The intertwined physics of active chemical

- reactions and phase separation, *Curr. Opin. Colloid Interface Sci* **61**, 101606 (2022).
- [23] J. W. Gibbs, On the Equilibrium of Heterogeneous Substances, *Trans. Conn. Acad. Arts Sci* **3**, 108 (1876).
- [24] D. Zwicker and L. Laan, Evolved interactions stabilize many coexisting phases in multicomponent liquids, *Proc. Natl. Acad. Sci. U.S.A.* **119**, e2201250119 (2022).
- [25] R. Bellman, *Introduction to Matrix Analysis: Second Edition* (SIAM, 1997).
- [26] Y. Qiang and D. Zwicker, *Flory: A Python package for finding coexisting phases in multicomponent mixtures* (2025).
- [27] Z. Mester, N. A. Lynd, and G. H. Fredrickson, Numerical self-consistent field theory of multicomponent polymer blends in the Gibbs ensemble, *Soft Matter* **9**, 11288 (2013).
- [28] F. Schmid, Self-consistent-field theories for complex fluids, *J. Phys.: Condens. Matter* **10**, 8105 (1998).
- [29] A. Z. Panagiotopoulos, Gibbs Ensemble Techniques, in *Observation, Prediction and Simulation of Phase Transitions in Complex Fluids*, Nato Science Series C, edited by M. Baus, L. F. Rull, and J.-P. Ryckaert (Springer Netherlands, Dordrecht, 1995) pp. 463–501.
- [30] B. Smit and D. Frenkel, Calculation of the chemical potential in the Gibbs ensemble, *Molecular Physics* **68**, 951 (1989).
- [31] D. Qian, T. C. T. Michaels, and T. P. J. Knowles, Analytical Solution to the Flory–Huggins Model, *J. Phys. Chem. Lett.* **13**, 7853 (2022).
- [32] N. A. Erkamp, M. A. M. Verwiel, D. Qian, T. Sneideris, F. A. Spaepen, D. A. Weitz, J. C. M. van Hest, and T. P. J. Knowles, Biomolecular condensates with complex architectures via controlled nucleation, *Nat Chem Eng* **1**, 430 (2024).
- [33] N. Rostam, S. Ghosh, C. F. W. Chow, A. Hadarovich, C. Landerer, R. Ghosh, H. Moon, L. Hersemann, D. M. Mitrea, I. A. Klein, A. A. Hyman, and A. Toth-Petroczy, CD-CODE: Crowdsourcing condensate database and encyclopedia, *Nat Methods* **20**, 673 (2023).
- [34] J. Kirschbaum and D. Zwicker, Controlling biomolecular condensates via chemical reactions, *Journal of The Royal Society Interface* **18**, 20210255 (2021).
- [35] J. Söding, D. Zwicker, S. Sohrabi-Jahromi, M. Boehning, and J. Kirschbaum, Mechanisms for Active Regulation of Biomolecular Condensates, *Trends in Cell Biology* **30**, 4 (2020).
- [36] C. A. Weber, D. Zwicker, F. Jüllicher, and C. F. Lee, Physics of active emulsions, *Rep. Prog. Phys.* **82**, 064601 (2019).
- [37] C. Luo, Y. Qiang, and D. Zwicker, Beyond pairwise: Higher-order physical interactions affect phase separation in multicomponent liquids, *Phys. Rev. Res.* **6**, 033002 (2024).
- [38] F. Chen and W. M. Jacobs, Programmable phase behavior in fluids with designable interactions, *The Journal of Chemical Physics* **158**, 214118 (2023).
- [39] D. Qian, H. Ausserwoger, W. E. Arter, R. M. Scrutton, T. J. Welsh, T. Kartanas, N. Ermann, S. Qamar, C. Fischer, T. Sneideris, P. S. George-Hyslop, R. V. Pappu, and T. P. J. Knowles, *Linking modulation of bio-molecular phase behaviour with collective interactions* (2023).
- [40] H. R. Kilgore, I. Chinn, P. G. Mikhael, I. Mitnikov, C. Van Dongen, G. Zylberberg, L. Afeyan, S. F. Bani, S. Wilson-Hawken, T. I. Lee, R. Barzilay, and R. A. Young, Protein codes promote selective subcellular compartmentalization, *Science* **0**, eadq2634 (2025).
- [41] I. R. Graf and B. B. Machta, Thermodynamic stability and critical points in multicomponent mixtures with structured interactions, *Phys. Rev. Res.* **4**, 033144 (2022).
- [42] R. B. Teixeira, G. Carugno, I. Neri, and P. Sartori, *Liquid Hopfield model: Retrieval and localization in heterogeneous liquid mixtures* (2023), arXiv:2310.18853 [cond-mat, physics:physics, q-bio].

Appendix A: Simulation details

1. Continuous field theory

The continuous simulations shown in Fig. 1 of the main text are based on a spatially averaged form of the non-dimensional free energy density in Eq. (2), extended with the interfacial energy to penalize sharp interfaces,

$$\bar{f}_{\text{spatial}} = \frac{1}{V} \int \left[\frac{1}{2} \sum_{i,j=1}^{N_c} \chi_{ij} \phi_i \phi_j + \sum_{i=1}^{N_c} \phi_i \ln \phi_i + \frac{1}{2} \ell^2 \sum_{i=1}^{N_c} |\nabla \phi_i|^2 \right] d\mathbf{r}, \quad (\text{A1})$$

where V is the volume of the system and ℓ is the interfacial width. The evolution of the conserved volume fraction fields ϕ_i then follows the Cahn-Hilliard equation

$$\frac{\partial \phi_i}{\partial t} = \nabla \cdot \sum_{j=1}^{N_c} \Lambda_{ij} \nabla \mu_j, \quad (\text{A2})$$

where $\mu_i = V \delta \bar{f}_{\text{spatial}} / \delta \phi_i$ is the non-dimensional chemical potential of each component, and Λ_{ij} is the mobility matrix selected to satisfy the incompressibility $\sum_i \phi_i = 1$ [20]. Specifically, we choose

$$\Lambda_{ij} = \lambda (\phi_i \delta_{ij} - \phi_i \phi_j). \quad (\text{A3})$$

The mobility matrix has no influence on coexisting phases in the stationary state, while the interfacial term proportional to ℓ only mildly modifies the coexisting concentrations via Laplace pressure effects [20].

We obtained the metastable states in Fig. 1 by numerically solving Eq. (A2) from various initial states. We generate initial states by adding random noise to the homogeneous state followed by adjustments to satisfy the incompressibility. A semi-implicit method is used to improve the numerical stability. For all the simulations, we use $\ell = 4$, $\lambda = 1$ and a periodic 2D simulation box of 64×64 .

2. Stability of the homogeneous state

The stability of the homogeneous state is governed by the eigenvalues of the Hessian matrix H_{ij} of the free energy given by Eq. (1) in the main text,

$$H_{ij} = \frac{\partial^2 f}{\partial \bar{\phi}_i \partial \bar{\phi}_j} = \chi_{ij} + \frac{\delta_{ij}}{\bar{\phi}_i} - \chi_{1j} - \chi_{i1} + \frac{1}{\bar{\phi}_1}, \quad (\text{A4})$$

with $i, j \in [2, N_c]$. Note that $\mathbf{H} = \{H_{ij}\}_{i,j=2}^{N_c}$ is a $(N_c - 1)$ -dimensional matrix since we removed the dependency on $\bar{\phi}_1$, using the incompressibility condition $\bar{\phi}_1 = 1 - \sum_{i=2}^{N_c} \bar{\phi}_i$. To obtain numerical estimates, we simply sample matrices and diagonalize them numerically.

3. Numerical algorithm for finding coexisting phases

There are multiple challenges for determining coexisting phases in equilibrium in multicomponent mixture: First, the optimization problem is high-dimensional. Second, different types of constraints, such as incompressibility and volume conservation, need to be satisfied. In addition, it is generally difficult to conclude whether the obtained phase-separated states with multiple coexisting phases are the true equilibrium or metastable states due to multistability.

In a previous publication [24], we designed an efficient algorithm to obtain coexisting phases by exchanging components between compartments, guided by thermodynamic properties such as osmotic pressure and chemical potential. To achieve high performance, the constraint of volume conservation was relaxed, making it difficult to uniformly sample the entire phase diagram [24]. This flaw in sampling, as well as a small number of compartments, might have biased the result toward metastable states instead of the true equilibrium, which was highlighted in Ref. [16]. To circumvent these challenges, we designed an improved method based on a free energy optimization strategy inspired by polymeric field theories [28], where the volume conservation is automatically guaranteed by introducing conjugate fields. Our method is now publicly available [26].

Instead of solving the balance equations of chemical potentials and osmotic pressures, we adopt the more fundamental idea of free energy minimization, which is the origin of the balance equations. The equilibrium coexisting phases can be obtained by optimizing the average free energy density given by Eq. (2) in the main text over all possible phase counts and phase compositions. To allow different phase counts, we consider an ensemble of M abstract compartments as proposed in Ref. [24], where M is much larger than the number of components N_c . To alleviate the problem of negative volume fractions during the relaxation dynamics and conserve the average volume fractions, we extend the free energy of Eq. (2) into the form

$$\bar{f} = \sum_{m=1}^M J_m \left[\frac{1}{2} \sum_{i,j=1}^{N_c} \chi_{ij} \phi_i^{(m)} \phi_j^{(m)} - \sum_{i=1}^{N_c} w_i^{(m)} \phi_i^{(m)} + \xi_m \left(\sum_{i=1}^{N_c} \phi_i^{(m)} - 1 \right) \right] - \sum_{i=1}^N \bar{\phi}_i \ln Q_i + \eta \left(\sum_{m=1}^M J_m - 1 \right), \quad (\text{A5})$$

with the single molecule partition function

$$Q_i = \sum_{m=1}^M J_m \exp \left(-w_i^{(m)} \right). \quad (\text{A6})$$

Here, J_m are the relative volumes of the compartments, $w_i^{(m)}$ are the conjugate variables of $\phi_i^{(m)}$, and ξ_m and η are the Lagrangian multipliers for incompressibility of each compartment and compartment volume conservation, respectively. Consequently, the extremum of Eq. (A5) with respect to $\xi(x)$ corresponds to incompressibility,

$$\frac{\partial \bar{f}}{\partial \xi_m} \propto \left(\sum_{i=1}^{N_c} \phi_i^{(m)} - 1 \right) J_m = 0 \quad \Rightarrow \quad \sum_{i=1}^{N_c} \phi_i^{(m)} = 1, \quad (\text{A7})$$

the extremum with respect to η corresponds to conservation of the total volume of all compartments,

$$\frac{\partial \bar{f}}{\partial \eta} \propto \sum_{m=1}^M J_m - 1 = 0 \quad \Rightarrow \quad \sum_{m=1}^M J_m = 1, \quad (\text{A8})$$

and the extremum with respect to $w_i^{(m)}$ defines the relationship between $\phi_i^{(m)}$ and $w_i^{(m)}$,

$$\frac{\partial \bar{f}}{\partial w_i^{(m)}} \propto -\phi_i^{(m)} J_m + \frac{\bar{\phi}_i}{Q_i} \exp(-w_i^{(m)}) J_m = 0 \quad \Rightarrow \quad \phi_i^{(m)} = \frac{\bar{\phi}_i}{Q_i} \exp(-w_i^{(m)}). \quad (\text{A9})$$

By inserting Eqs. (A7)–(A9) into Eq. (A5), Eq. (2) is recovered except for a constant, which has no influences on thermodynamics. Therefore, minimizing Eq. (A5) will naturally lead to balanced chemical potentials and osmotic pressures, and it is unnecessary to consider them explicitly. To optimize the free energy density given by Eq. (A5), we obtain the self-consistent equations

$$1 = \sum_{i=1}^{N_c} \phi_i^{(m)} \quad (\text{A10a})$$

$$1 = \sum_{m=1}^M J_m \quad (\text{A10b})$$

$$\phi_i^{(m)} = \frac{\bar{\phi}_i}{Q_i} \exp(-w_i^{(m)}) \quad (\text{A10c})$$

$$w_i^{(m)} = \sum_{j=1}^{N_c} \chi_{ij} \phi_j^{(m)} + \xi_m \quad (\text{A10d})$$

$$-\eta = \frac{1}{2} \sum_{i,j=1}^{N_c} \chi_{ij} \phi_i^{(m)} \phi_j^{(m)} - \sum_{i=1}^{N_c} w_i^{(m)} \phi_i^{(m)} + \xi_m \left(\sum_{i=1}^{N_c} \phi_i^{(m)} - 1 \right) - \sum_{i=1} \phi_i^{(m)}. \quad (\text{A10e})$$

To solve these equations, we design the following iterative scheme

$$Q_i^{(m)} = \sum_{m=1}^M \exp(-w_i^{(m)}) J_m \quad (\text{A11a})$$

$$\phi_i^{(m)} = \frac{\bar{\phi}_i}{Q_i^{(m)}} \exp(-w_i^{(m)}) \quad (\text{A11b})$$

$$\xi_m = \frac{1}{N_c} \left(\sum_{i=1}^{N_c} w_i^{(m)} - \sum_{i,j=1}^{N_c} \chi_{ij} \phi_j^{(m)} \right) \quad (\text{A11c})$$

$$\eta_m = -\frac{1}{2} \sum_{i,j=1}^{N_c} \chi_{ij} \phi_i^{(m)} \phi_j^{(m)} + \sum_{i=1}^{N_c} w_i^{(m)} \phi_i^{(m)} - \xi_m \left(\sum_{i=1}^{N_c} \phi_i^{(m)} - 1 \right) + \sum_{i=1} \phi_i^{(m)} \quad (\text{A11d})$$

$$\bar{\eta} = \sum_{m=1}^M \eta_m J_m \quad (\text{A11e})$$

$$w_i^{(m)*} = \sum_{j=1}^{N_c} \chi_{ij} \phi_j^{(m)} + \xi^{(m)} \quad (\text{A11f})$$

$$J_m^* = J^{(m)} + \eta^{(m)} - \bar{\eta}, \quad (\text{A11g})$$

where the asterisks denote the output of the iteration. In order to improve numerical stability, we also adopt the simple mixing strategy,

$$w_i^{(m),\text{new}} = w_i^{(m)} + \alpha \left(w_i^{(m)*} - w_i^{(m)} \right) \quad (\text{A12a})$$

$$J^{(m),\text{new}} = J_m + \beta (J_m^* - J_m), \quad (\text{A12b})$$

where α and β are two empirical constants, which are usually chosen near 10^{-3} . We note again that in such iteration scheme the problem of negative volume fractions is relieved. However, there is no guarantee that relative compartment volume J_m is always positive. Although the algorithm does not suffer from negative J_m , negative J_m implies that the system might be outside of the allowed region on the tie hyperplane. To alleviate this, we always use β smaller than α , and adopt a killing-and-revive strategy to correct the worst cases: Once J_m is found to be negative at certain m , e.g. m_0 , the corresponding compartment is considered “dead” and is going to be revived by resetting J_{m_0} to its initial value, and the corresponding $w_i^{(m_0)}$ will be redrawn from random distributions. To obey volume conservation, all other J_m will be renormalized. The same scheme is used to initialize the simulation, i.e., all compartments are considered “dead” at the beginning of the simulation.

Due to multistability, this algorithm does not guarantee that the true equilibrium state is always found. Since pairwise exchange of volume fractions is replaced by a global redistribution, the new numerical method has lower time complexity with respect to the number of compartments M compared to the method in Ref. [24]. Therefore we handle the problem of multistability by launching many more compartments than the number of components, $M \gg N_c$. In all our numerical results, the number of compartments are at least $M = 16N_c$. We justified this choice by increasing number of compartments until both the number and the compositions of unique coexisting phases do not change. Under such setting, the equilibrium coexisting phases are prominently obtained.

Appendix B: Identical interactions and symmetric composition

In this section, we first derive the stability condition for mixtures with identical interactions, $\chi_{ij} = \bar{\chi}(1 - \delta_{ij})$, and symmetric composition, $\bar{\phi}_i = 1/N_c$. Then in B2, we provide a sufficient condition for the equilibrium state with multiple coexisting phases. In B3, we derive the analytical approximation of the volume fraction of the dilute component in each of the coexisting phases. In B4, we justify the assumption for the compositions of the coexisting phases in B2 for completeness.

1. Stability analysis of homogeneous states

With identical interactions and symmetric composition, the Hessian given by Eq. (A4) reads $H_{ij} = (\delta_{ij} + 1)(N_c - \chi)$, which has two unique eigenvalues $N_c - \chi$ and $N_c(N_c - \chi)$. The homogeneous state is unstable when the Hessian above is no longer positive definite, i.e., when $\bar{\chi} > N_c$; see the blue line in Fig. A1.

2. Sufficient condition for the equilibrium phase-separated state

To obtain the sufficient condition for the state with multiple coexisting phases to be stable, we first derive the free energy of the homogeneous state. With identical interactions and symmetric composition, the free energy density given by Eq. (1) reads

$$f = \frac{N_c - 1}{2N_c} \bar{\chi} - \ln N_c. \quad (\text{A1})$$

Since all components interact equally, coexisting phases must have permutational symmetry. Each phase then enriches one component with volume fraction $\phi_h = 1 - (N_c - 1)\phi_1$, while all other components have the same volume fraction ϕ_1 . In principle, there could also be coexisting phases that enrich more components per phase, but we will show in B4 that the state above is the energetically preferred phase-separated state when $\bar{\chi}$ is increased. For this state, the free energy density in each phase reads

$$f(\phi_1) = (N_c - 1)\bar{\chi}\phi_h\phi_1 + \frac{(N_c - 1)(N_c - 2)}{2}\bar{\chi}\phi_1^2 + \phi_h \ln \phi_h + (N_c - 1)\phi_1 \ln \phi_1. \quad (\text{A2})$$

Note that Eq. (A2) reduces to Eq. (A1) in the homogeneous case when $\phi_h = \phi_1 = 1/N_c$. Since all coexisting phases have the same free energy density due to permutational symmetry, the coexisting phases are energetically favored over the homogeneous state if the minimal value of Eq. (A2) is lower than that of the homogeneous state given by Eq. (A1). The orange curve in Fig. A1 shows the results from a numerical minimization of Eq. (A2) compared to Eq. (A1). To obtain an analytical approximation of the minimal interaction strength necessary for phase separation, we note that with $\phi_1 \rightarrow +0$, the free energy $f(\phi_1) \rightarrow 0$, while its derivative $df(\phi_1)/d\phi_1 \rightarrow -\infty$. Using the mean

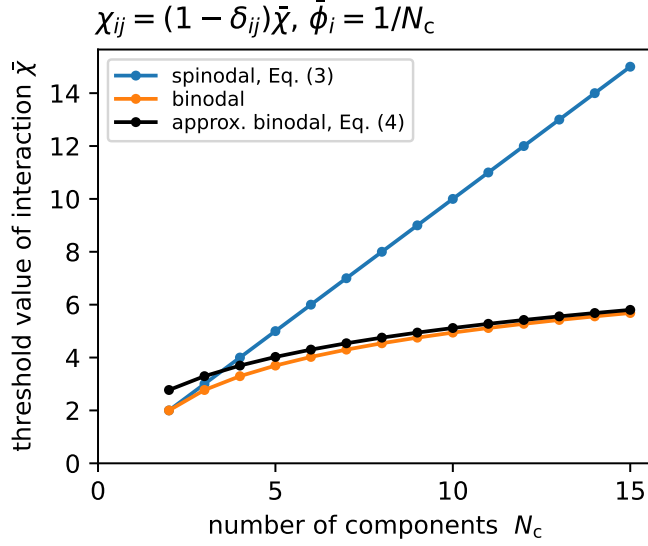


FIG. A1. **Interaction strength for stable multiphase coexistence differs from stability analysis in mixtures with identical interactions and symmetric composition.** A homogeneous mixture is unstable for interactions $\bar{\chi}$ above the spinodal (blue line, given by Eq. (3) in the main text). In contrast, phase separation is energetically favorable for $\bar{\chi}$ above the binodal (orange line, obtained numerically). The black line shows the analytical approximation given by Eq. (4) in the main text.

value theorem, we then conclude that Eq. (A2) will have a minimum lower than Eq. (A1) when $f(1/N_c)$ is positive, implying

$$\bar{\chi} > \frac{2N_c}{N_c - 1} \ln N_c, \quad (\text{A3})$$

which is Eq. (4) in the main text.

3. Volume fraction of the dilute component in coexisting phases

We further consider the volume fraction ϕ_1 of the dilute components in coexisting phases. Denoting by $\phi_1 = \phi^-$ the minimizer of Eq. (A2), ϕ^- satisfies the equation

$$\bar{\chi} = \frac{1}{1 - N_c \phi^-} \left(\ln [1 - (N_c - 1)\phi^-] - \ln \phi^- \right). \quad (\text{A4})$$

Assuming that ϕ^- is much smaller than $1/N_c$, we obtain

$$\phi^-(N_c) \approx -\frac{W_0[-e^{-\bar{\chi}}(N_c(\bar{\chi} - 1) + 1)]}{N_c(\bar{\chi} - 1) + 1}, \quad (\text{A5})$$

where $W_0(r)$ is the principal branch of the Lambert W function, which satisfies $W(r)e^{W(r)} = r$. When $\bar{\chi} \gg \ln N_c$, the equation above can be further simplified to

$$\phi^- \stackrel{\bar{\chi} \gg 1}{\approx} e^{-\bar{\chi}}, \quad (\text{A6})$$

which is independent of N_c . Note that Eq. (A6) also shows that the assumption $\phi^- \ll 1/N_c$ is valid when $\bar{\chi} \gg \ln N_c$.

4. Justification for each phase enriching one component

Here we show that with $\bar{\chi} \gg \ln N_c$, a system with identical interactions and symmetric composition will minimize its free energy by separating into phases where each phase concentrates one component. The argument comprises three steps:

a. The coexisting phases in equilibrium must have the same free energy density. This can be proved by contradiction: Assuming coexisting phases have different free energy densities in equilibrium, there must exist one of the coexisting phases with the lowest free energy density. Suppose such phase has a composition denoted by the vector $\phi = [\phi_1, \phi_2 \dots \phi_{N_c}]$, then a new collection of phases can be constructed by permuting the entries of the vector. Since all the interactions are identical, these phases share the same free energy density. Also the average composition of these phases is symmetric, meaning that the coexistence of all the phases in the collection becomes a possible candidate state for the equilibrium state of the mixture. Since this state has lower free energy density than the assumed state, the initial assumption of equilibrium is violated. Therefore, with identical interactions and symmetric composition, all coexisting phases in equilibrium must have the same free energy density.

b. Each component can either be dilute/concentrated in each of the coexisting phases. As a result of equal free energy density, the composition of the coexisting phases must be the local minimizer of the free energy function, otherwise a new set of coexisting phases with lower free energy can be found. Therefore, the compositions must satisfy $\partial f / \partial \phi_i = 0$ for $i = 2 \dots N_c$, which is the case for

$$-\bar{\chi}\phi_i + \ln \phi_i = \text{constant} \quad (\text{A7})$$

for $i = 1, 2 \dots N_c$, where the constant is the same across different components i . Since the function $g(\phi) = -\bar{\chi}\phi + \ln \phi$ can at most have two piecewise monotonic domains in $\phi \in (0, 1)$, the equation above can have at most two solutions, meaning that each component can either be dilute or concentrated, while all the dilute components share the same composition ϕ_l and all the concentrated components share the same composition ϕ_h .

c. Each of the coexisting phases prefers to concentrate only one component. Suppose the system would phase separate into phases that concentrate K components with volume fraction ϕ_h , then in each phase $N_c - K$ components are dilute and share the volume fraction ϕ_l , satisfying $K\phi_h + (N_c - K)\phi_l = 1$. Using Eq. (A7), we denote by $\phi_l = \phi^-(N_c)$ the volume fraction that minimizes the free energy, which satisfies

$$\bar{\chi} = \frac{\ln \phi_h - \ln \phi_l}{\phi_h - \phi_l}. \quad (\text{A8})$$

In the limit $\phi_l \ll 1$, we find

$$\phi_l \approx \frac{1}{K} e^{-K\bar{\chi}}. \quad (\text{A9})$$

Since the right hand side decreases monotonically with K for $\bar{\chi} > 0$, the dilute components become more dilute for larger K . For sufficient large value of $\bar{\chi}$, the concentrated components will take over the vast majority of the phase ($\phi_h \approx K^{-1}$), making these concentrated components effectively a subsystem of K components with equal interactions and volume fractions. This subsystem will undergo phase separation again since the homogeneous state is more prone to phase separation for fewer components; see Fig. A1. Taken together, the system prefers to enrich one component in each phase since the enriched components would otherwise phase separate from each other.

Combining the three steps above, in the case of identical interactions and symmetric average composition, we find that each of the coexisting phases must enrich exactly one component when the phase-separated state is the equilibrium state. Intuitively, all components dislike each other equally and they prefer to separate from each other when possible. Phases that enrich more components are not energetically preferred without other effects such as higher-ordered interactions [37].

Appendix C: Identical interactions and uniformly distributed composition

1. Average number of unstable modes

We here consider the number of unstable modes averaged over the entire phase diagram (random average composition satisfying $\sum_i \bar{\phi}_i = 1$) for identical interactions, $\chi_{ij} = \bar{\chi}(1 - \delta_{ij})$. The Hessian given by Eq. (A4) can be simplified and rewritten in matrix form,

$$\mathbf{H} = \text{diag} \left\{ \frac{1}{\bar{\phi}_i} - \chi \right\}_{i=2}^{N_c} + \left(\frac{1}{\bar{\phi}_1} - \chi \right) \mathbf{u}\mathbf{u}^T, \quad (\text{A1})$$

where \mathbf{u} is an all-one vector in $N_c - 1$ dimensions. The rank- n leading minor of \mathbf{H} , denoted by \mathbf{H}_n , reads

$$\mathbf{H}_n = \text{diag} \left\{ \frac{1}{\bar{\phi}_i} - \chi \right\}_{i=2}^{n+1} + \left(\frac{1}{\bar{\phi}_1} - \chi \right) \mathbf{u}_n \mathbf{u}_n^T, \quad (\text{A2})$$

with $n = 1, 2, \dots, N_c - 1$ and \mathbf{u}_n is a all-one vector in n dimensions. Making use of the Cauchy interlacing theorem, the number of negative eigenvalues of \mathbf{H} can be obtained by calculating the number of sign changes in the sequence

$$\det \mathbf{H}_0, \det \mathbf{H}_1, \dots, \det \mathbf{H}_{N_c-1}, \quad (\text{A3})$$

where $\det \mathbf{H}_0$ is defined to be 1. The terms $\det \mathbf{H}_n$ can be determined using the Weinstein-Aronszajn identity,

$$\begin{aligned} \det \mathbf{H}_n &= \left(\frac{1}{\bar{\phi}_1} - \chi \right)^n \det \text{diag} \left\{ \frac{\bar{\phi}_i^{-1} - \chi}{\bar{\phi}_1^{-1} - \chi} \right\}_{i=2}^{n+1} \det \left(\mathbf{I} + \mathbf{u}_n \mathbf{u}_n^T \text{diag} \left\{ \frac{\bar{\phi}_1^{-1} - \chi}{\bar{\phi}_i^{-1} - \chi} \right\}_{i=2}^{n+1} \right) \\ &= \prod_{i=1}^{n+1} \left(\frac{1}{\bar{\phi}_i} - \chi \right) \left(\sum_{i=1}^{n+1} \frac{1}{\frac{1}{\bar{\phi}_i} - \chi} \right). \end{aligned} \quad (\text{A4})$$

We here assume that $\bar{\phi}_i^{-1} \neq \chi$ since we are interested in the average behavior over the entire phase diagram, where the points violating this condition have zero measure. Since the number of negative eigenvalues is invariant if the matrix is permuted by both rows and columns at the same time, we can also require that sequence

$$\frac{1}{\bar{\phi}_1} - \chi, \frac{1}{\bar{\phi}_2} - \chi, \dots, \frac{1}{\bar{\phi}_{N_c}} - \chi \quad (\text{A5})$$

decreases monotonically. Comparing Eq. (A3) and Eq. (A4) with Seq. (A5), we obtain that the number of sign changes in Seq. (A3) can only be either (i) the number of negative elements in Seq. (A5), denoted by N_- , or (ii) one less, $N_- - 1$, since the term $\sum_{i=1}^{N_c} 1/(\bar{\phi}_i^{-1} - \chi)$ can at most change the sign once itself and cancel the sign changes of $\prod_{i=1}^{N_c} (\bar{\phi}_i^{-1} - \chi)$ once. We thus obtain the relationship between N_u and N_- given in the main text.

2. Bounds for number of coexisting phases with identical interactions

In the main text, the average number of coexisting phases over the entire phase diagram, \bar{N}_p , was obtained by constructing lower and upper bounds. For $N_c = 3$, the construction is visualized in Fig. 3 of the main text, and we now explain this construction for general N_c . For identical interactions, a state with K coexisting phases necessarily has $N_c - K$ non-phase-separating components (for the same reasons as discussed in section B4). The composition of these non-phase-separating components will be the same in all K coexisting phases, again due to identical interactions. The contribution of these components to the free energy density is thus identical in all phases, implying that these non-phase-separating components are effectively inert. The geometric interpretation is that all K -dimensional tie hyperplanes are parallel to one of the K -dimensional boundaries of the entire phase diagram. Assuming the total volume fractions of all non-phase-separating component are $\Delta\phi$, similar to Eq. (A8), we still obtain

$$\bar{\chi} = \frac{\ln \phi_h - \ln \phi_l}{\phi_h - \phi_l}, \quad (\text{A6})$$

where $\phi_h = 1 - \Delta\phi - (K-1)\phi_l$ is the volume fraction of the concentrated component of one phase, whereas ϕ_l is the volume fraction of all $K-1$ components that are diluted in this phase. Again assuming $\phi_l \ll 1/N_c$, we obtain the approximate solution

$$\phi_l \approx - \frac{W_0 \left[-e^{\Delta\phi(\bar{\chi}-1)} e^{-\bar{\chi}} (K(\bar{\chi}-1) + 1) \right]}{K(\bar{\chi}-1) + 1}. \quad (\text{A7})$$

Since W_0 is a monotonic increasing function, ϕ_l increases with larger $\Delta\phi$. This implies that increasing the volume fraction of non-phase-separating components disfavors phase separation, leading to higher concentration ϕ_l of the dilute component and lower concentration ϕ_h of the concentrated component in coexisting phases. Based on these monotonic dependencies, we construct upper bounds and lower bounds using the minimal and maximal value of ϕ_l of the real phase boundaries, which correspond to the outermost point and the innermost point of the phase boundaries in the real phase diagram.

Appendix D: Random interactions

1. Governing parameters for average phase count with random interactions

In the case of identical interactions, we obtained analytical governing parameters and asymptotic rules for the average number of unstable modes, \bar{N}_u , and average number of coexisting phases, \bar{N}_p ; see main text. In contrast, for

random interactions with zero mean, random matrix theories only grants us access to the governing parameter for \bar{N}_u , but it does not directly reveal anything about \bar{N}_p . To infer the governing parameter for \bar{N}_p , we exploit connections between the results from the other three known cases. For simplicity, we assume vanishing mean value of the random interactions in this section, unless specified otherwise.

To predict the scaling of \bar{N}_p with N_c and σ_χ , we first recall the results for \bar{N}_u for random interactions. Ignoring the sole outlier in the spectrum of the Hessian matrix given by Eq. (A4), the average number of negative eigenvalues is approximately the number of eigenvalues of the interaction matrix χ_{ij} smaller than $-1/\bar{\phi}_i = -N_c$, when $\bar{\phi}_i = 1/N_c$. In the case of asymmetric composition, the eigenvalue spectrum will be expanded, but in the limit of larger interaction variance, the shape of the spectrum is still dominated by the random interaction matrix [11]. In addition, we expect that this spectrum expansion has no preference for positive or negative values and thus averages out when we consider the average behavior over the entire phase diagram $\sum_i \bar{\phi}_i = 1$. Therefore, to find the governing parameters, we check the situation of symmetric composition and hypothesize that the result generalizes to the average behavior over the entire phase diagram. Denoting the eigenvalues of χ_{ij} by λ_k with $k = 1, 2 \dots N_c - 1$, the number of unstable modes, \bar{N}_u , can be roughly estimated by

$$\bar{N}_u \approx E_{N_c}[\lambda_k > \bar{\phi}_i^{-1}] \quad \text{for} \quad \chi_{ij} \sim \mathcal{N}(0, \sigma_\chi). \quad (\text{A1})$$

Since λ_k is distributed according to a semicircle law with radius $2\sigma_\chi\sqrt{N_c}$, we set $\lambda_k = 2\sigma_\chi\sqrt{N_c}\gamma$, where γ is a random variable according to a semicircle law with unit radius. We thus obtain $\bar{N}_u \approx E_{N_c}[2\sigma_\chi\sqrt{N_c}\gamma > \bar{\phi}_i^{-1}] = E_{N_c}[\gamma > \sqrt{N_c}/\sigma_\chi]$, indicating that \bar{N}_u is governed by the $\sigma_\chi/\sqrt{N_c}$ when $\chi_{ij} \sim \mathcal{N}(0, \sigma_\chi)$. However, even though this derivation is only approximative, the literature [11] and our numerical data shown in Fig. 4(a) of the main text suggest that the governing parameter is still valid when \bar{N}_u is obtained for a uniform average over the entire phase diagram.

Although Eq. (A1) provides no direct information about \bar{N}_p , it strikingly shares the same form as the relations for \bar{N}_u for identical interactions $\chi_{ij} \sim \mathcal{N}(\bar{\chi}, 0)$, allowing us to build a connection with \bar{N}_p by analogy. From Eq. (8) and Eq. (10) in the main text, we obtain

$$\bar{N}_u \approx E_{N_c}[\bar{\phi}_i > \bar{\chi}^{-1}] = E_{N_c}[\bar{\chi} > \bar{\phi}_i^{-1}] \quad \text{for} \quad \chi_{ij} \sim \mathcal{N}(\bar{\chi}, 0) \quad (\text{A2a})$$

$$\bar{N}_p \approx E_{N_c}[\bar{\phi}_i > e^{-\bar{\chi}}] = E_{N_c}[e^{\bar{\chi}} > \bar{\phi}_i^{-1}] \quad \text{for} \quad \chi_{ij} \sim \mathcal{N}(\bar{\chi}, 0). \quad (\text{A2b})$$

Note that $\bar{\chi}$ is tightly related to the eigenvalues, since in the case of identical interactions the relevant eigenvalues are all equal to $-\bar{\chi}$. The only difference between the unstable modes and the phase count in the equations above is that the interaction $\bar{\chi}$ is modified to $e^{\bar{\chi}}$. Inspired by this, we speculate that such a modification can also be applied to the case of random interactions, $\chi_{ij} \approx \mathcal{N}(0, \sigma_\chi)$. We thus propose

$$\bar{N}_p \approx E_{N_c}[e^{\lambda_k} > \bar{\phi}_i^{-1}] \quad \text{for} \quad \chi_{ij} \sim \mathcal{N}(0, \sigma_\chi). \quad (\text{A3})$$

Since $\lambda_k = 2\sigma_\chi\sqrt{N_c}\gamma$, and the average value of $\bar{\phi}_i$ is $1/N_c$, we further propose that $\bar{N}_p \approx E_{N_c}[2\sigma_\chi\sqrt{N_c}\gamma > \ln N_c]$. It leads to the governing parameter $\sigma_\chi\sqrt{N_c}/\ln N_c$, which we verified numerically in the main text.

2. Verification of the numerically estimated master functions

To confirm the scalings proposed in Eq. (11) in the main text, and the associated master functions shown in Fig. 5, we calculate the relative standard deviations across the selected number of components. Fig. A2a shows that the deviation between the true values of $(\bar{N}_u + 1)/N_c$ and the values predicted by the master function g_u is below 5% in the relevant parameter regime of repulsive interactions ($\bar{\chi} > 0$). Fig. A2b shows that the deviation is even smaller for the phase count \bar{N}_p/N_c , showing that it is incredibly well explained by the master function g_p for positive $\bar{\chi}$. In both datasets, the relative deviation is higher in the lower left corner of the plot ($\bar{\chi} < 0$ and small σ_χ). This is expected since most cases exhibit a homogeneous system, so the number of unstable modes is close to 0, while number of coexisting phases is close to 1. In these cases, the relative standard deviation degenerates to the standard deviation of the $1/N_c$, which is apparently high with respect to $1/N_c$ itself.

To validate our result further, we repeat the same procedure for determining the master functions using half the component count N_c everywhere. The respective deviations are very similar (compare Fig. A2 and Fig. A4), and comparing Fig. A3 of the main text to Fig. 5 shows that the resulting master functions are very similar. Taken together, this suggests that the master functions shown in Fig. A3 are reliable.

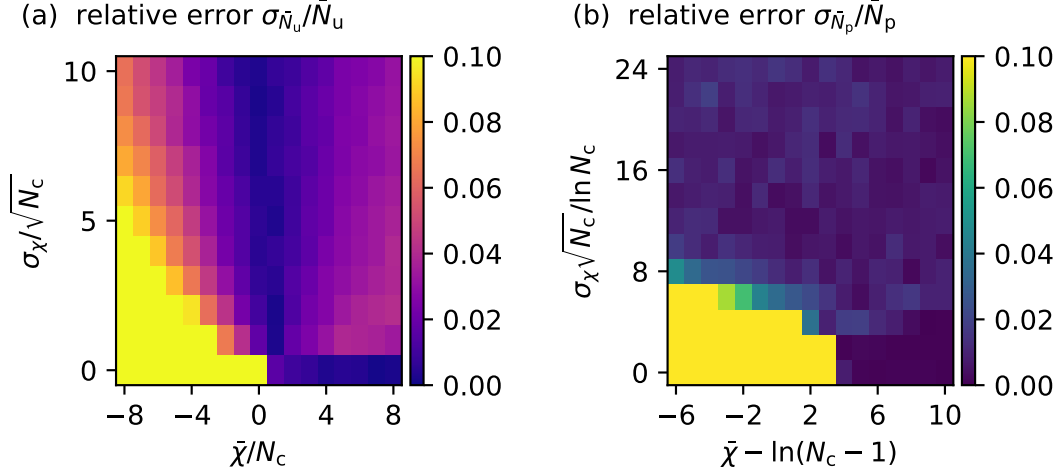


FIG. A2. **Relative standard deviation of the numerically estimated master functions for $N_c \in [16, 32]$.** (a) Relative standard deviation of number of unstable modes, $\sigma_{\bar{N}_u}/\bar{N}_u$, and (b) relative standard deviation of number of coexisting phases, $\sigma_{\bar{N}_p}/\bar{N}_p$, as a function of two scaling variables (a) $\bar{\chi}/N_c$ and $\sigma_\chi/\sqrt{N_c}$, and (b) $\bar{\chi} - \ln(N_c - 1)$ and $\sigma_\chi\sqrt{N_c}/\ln N_c$, respectively. Note that the relative error in the left corner of both panels is high while the absolute error is still low, since the reference values $\bar{N}_u \approx 0$ and $\bar{N}_p \approx 1$ are very low in this region. Standard deviations are calculated for $N_c = 16, 20, 24, 28, 32$.

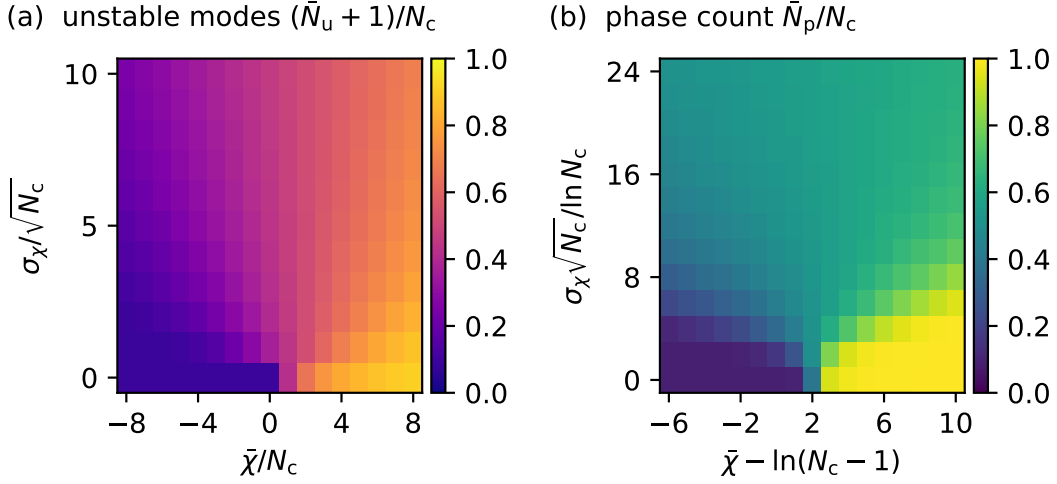


FIG. A3. **Numerically estimated master functions for $N_c \in [8, 16]$.** Data are averaged over $N_c = 8, 10, 12, 14, 16$. 300-3000 random pairs of interaction matrices and compositions are drawn for each fixed N_c , $\bar{\chi}$ and σ_χ . Other elements are the same as Fig. 5 in the main text.

3. Linear regime of average unstable modes/coexisting phases count with respect to mean interaction

The master functions g_u and g_p shown in Fig. A3 in the main text were only estimated numerically. However, their smooth behavior in the region of large σ_χ and small $\bar{\chi}$ suggests that there is a simpler relationship in this region. To obtain such a relationship, we investigate deviations from the line for $\bar{\chi} = 0$ for small $|\bar{\chi}|$.

For the unstable modes, $(\bar{N}_u + 1)/N_c$, such relationship can be inferred again from random matrix theory. The eigenvalues of the random interaction matrix are distributed according to the semicircle law with radius $r = 2\sigma_\chi\sqrt{N_c}$. Adding a mean value $\bar{\chi}$ shifts the distribution by $-\bar{\chi}$ accordingly. Therefore, the normalized number of unstable modes will increase roughly by $2r\bar{\chi}/(\pi r^2) = \bar{\chi}/(\pi\sigma_\chi\sqrt{N_c})$ when $\bar{\chi} \ll \sigma_\chi\sqrt{N_c}$. This means $\bar{\chi}$ leads to a linear correction of $(\bar{N}_u + 1)/N_c$. Fig. A5 shows that such a shift collapses the data for various $\bar{\chi}$. Note that the shift $\bar{\chi}/(\pi\sigma_\chi\sqrt{N_c})$ can

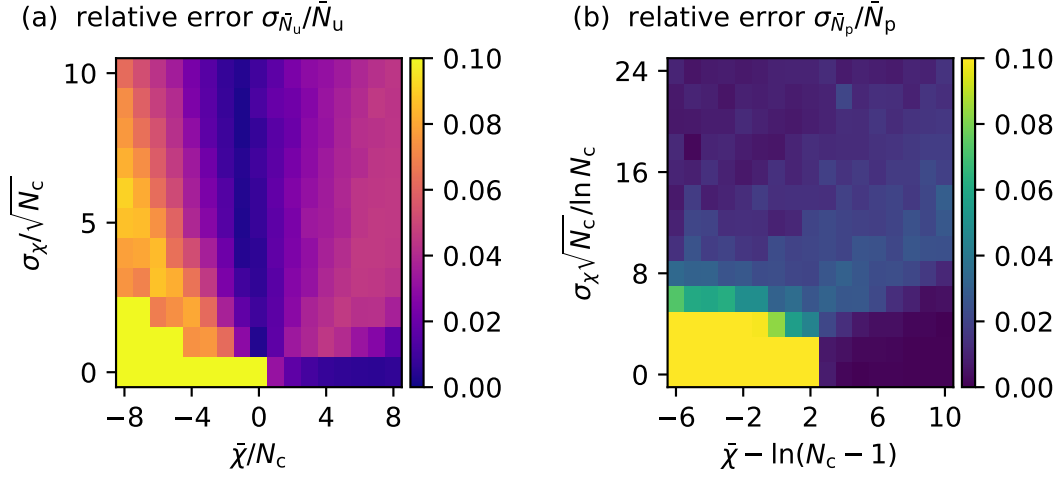


FIG. A4. **Relative standard deviation of the numerically estimated of master functions for $N_c \in [8, 16]$.** Standard deviations are calculated for $N_c = 8, 10, 12, 14, 16$. 300-3000 samples of random interaction matrices and compositions are drawn for each fixed N_c , $\bar{\chi}$ and σ_χ . Other elements are the same as Fig. A2.

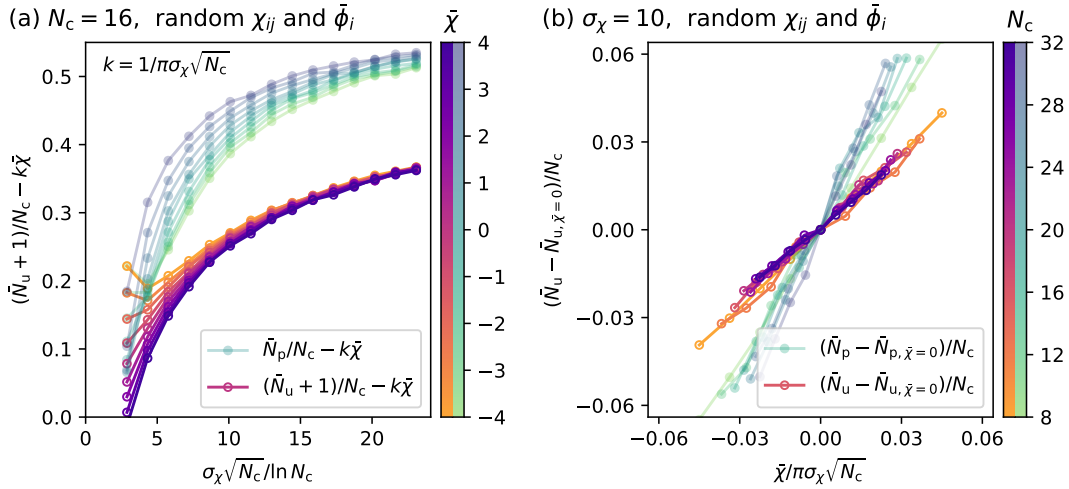


FIG. A5. **Linear correction proportional to $\bar{\chi}$ collapses data of the number of unstable modes.** (a) Shifted normalized average number of unstable modes (orange-purple) and coexisting phases (green-blue) as a function of the scaled standard deviation of the interactions for various mean interactions $\bar{\chi}$ at fixed component count $N_c = 16$. The shift coefficient $k = 1/\pi\sigma_\chi\sqrt{N_c}$. (b) Changes in the normalized average number of unstable modes (orange-purple) and coexisting phases (green-blue) as a function of the scaled mean interactions for various component counts N_c at fixed standard deviation of the interactions, $\sigma_\chi = 10$.

be interpreted as the ratio between the governing parameter for $(\bar{N}_u + 1)/N_c$ in the identical interaction case, $\bar{\chi}/N_c$, and that in the zero-mean random interaction case, $\sigma_\chi/\sqrt{N_c}$.

We speculate that a similar linear relationship with respect to $\bar{\chi}$ holds for the phase count \bar{N}_p/N_c . By comparing the governing parameters $\bar{\chi} - \ln(N_c - 1)$ and $\sigma_\chi\sqrt{N_c}/\ln N_c$, we conclude that the shift is proportional to $\bar{\chi} \ln(N_c)/(\sigma_\chi\sqrt{N_c})$. We also include a fitting parameter λ since we have little knowledge of the analytical form of g_p , in contrast to g_u . Fig. A6a shows that shifting the \bar{N}_p/N_c data according to $\lambda\bar{\chi} \ln(N_c)/(\sigma_\chi\sqrt{N_c})$ collapses the data for various $\bar{\chi}$ over a broad range. The fitting parameter is chosen to be 0.2, independent of N_c (Fig. A6b). Note that these two linear relationships indicate that in the large N_c limit, the influences of mean interaction $\bar{\chi}$ is subtle, since both $1/(\pi\sigma_\chi\sqrt{N_c})$ and $\ln N_c/\sqrt{N_c}$ are vanishingly small with large N_c , consistent with Fig. 5 in the main text.

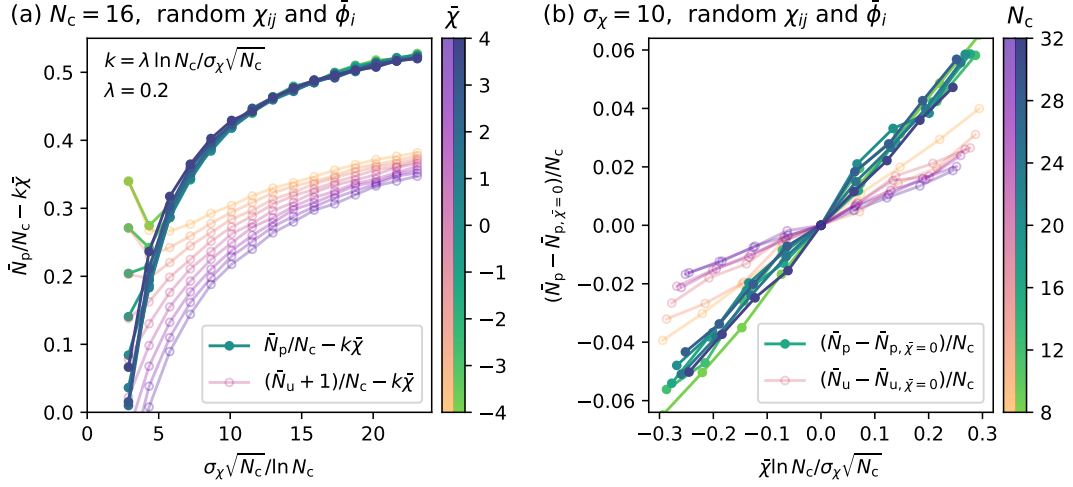


FIG. A6. **Linear correction proportional to $\bar{\chi}$ collapses data of the number of coexisting phases.** (a) Shifted normalized average number of unstable modes (orange-purple) and coexisting phases (green-blue) as a function of the scaled standard deviation of the interactions for various mean interactions $\bar{\chi}$ at fixed component count $N_c = 16$. The shift coefficient $k = \lambda \ln N_c / \sigma_\chi \sqrt{N_c}$, where λ is a fitting constant independent of N_c . (b) Changes in the normalized average number of unstable modes (orange-purple) and coexisting phases (green-blue) as a function of the scaled mean interactions for various component counts N_c at fixed standard deviation of the interactions, $\sigma_\chi = 10$.

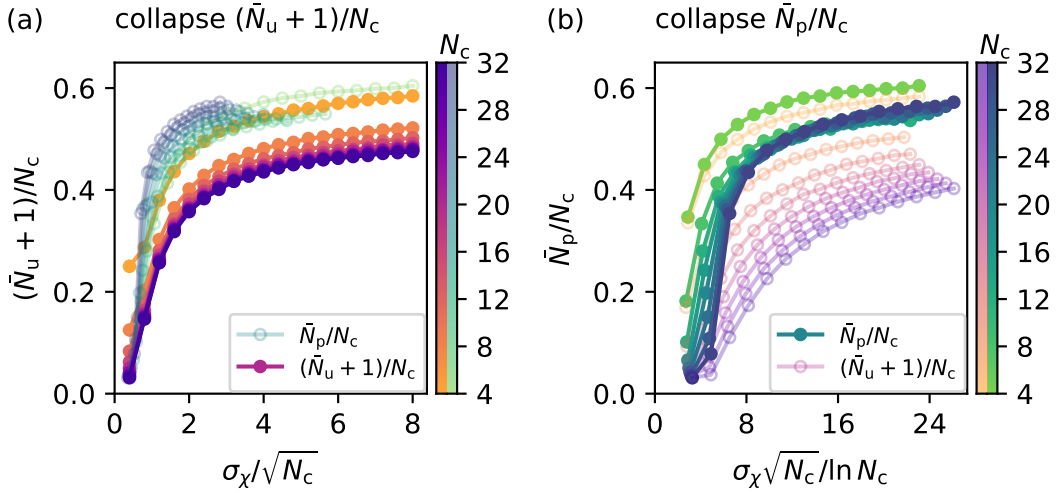


FIG. A7. **Average number of unstable modes and coexisting phases with random interactions but symmetric compositions.** Normalized average number of unstable modes, $(\bar{N}_u + 1)/N_c$ (orange-purple), and normalized average number of coexisting phases, \bar{N}_p/N_c (green-blue), as a function of two different scalings of the standard deviation σ_χ of the interactions for various component counts N_c and $\bar{\chi} = 0$. Each dot results from an average over 10^3 – 10^4 pairs of random interaction matrices χ_{ij} . The composition is fixed at $\bar{\phi}_i = N_c$.

4. Validation of the scaling laws at the center of the phase diagram

In the main text, we have averaged the phase count N_p and the number N_u of unstable modes for random interactions uniformly over the entire phase diagram. To test whether our derived scaling laws hold more generally, we also consider two other sampling methods: First, we sample the boundary of the phase diagram uniformly, which effectively reduces the system to a system with $N_c - 1$ components, leaving all scaling laws unchanged when $N_c \gg 1$. Second, we only sample the center of the phase diagram at the symmetric compositions $\bar{\phi}_i = 1/N_c$, where the scaling laws also still

hold (Fig. A7). These scalings are also consistent with the earlier results for equal interactions given in Eqs. (3) and (4). Note that the scaling for \bar{N}_u in this case is a direct result of random matrix theory [8]. Taken together, these results suggest that the obtained scaling laws are not sensitive to the details of the composition sampling. In particular, the observed discrepancy between N_p and N_u reflects a general behavior of multicomponent mixtures.